

Unveiling the Nature of Pt Single-Atom Catalyst during Electrocatalytic Hydrogen Evolution and Oxygen Reduction Reactions

Junjie Li, Mohammad Norouzi Banis, Zhouhong Ren, Keegan R. Adair, Kieran Doyle-Davis, Debora Motta Meira, Y. Zou Finfrock, Lei Zhang, Fanpeng Kong, Tsun-Kong Sham, Ruying Li, Jun Luo, and Xueliang Sun*

Single-atom catalysts (SACs) have attracted significant attention due to their superior catalytic activity and selectivity. However, the nature of active sites of SACs under realistic reaction conditions is ambiguous. In this work, high loading Pt single atoms on graphitic carbon nitride (g-C₃N₄)-derived N-doped carbon nanosheets (Pt₁/NCNS) is achieved through atomic layer deposition. Operando X-ray absorption spectroscopy (XAS) is performed on Pt single atoms and nanoparticles (NPs) in both the hydrogen evolution reaction (HER) and oxygen reduction reaction (ORR). The operando results indicate that the total unoccupied density of states of Pt 5d orbitals of Pt₁ atoms is higher than that of Pt NPs under HER condition, and that a stable Pt oxide is formed during ORR on Pt₁/NCNS, which may suppress the adsorption and activation of O₂. This work unveils the nature of Pt single atoms under realistic HER and ORR conditions, providing a deeper understanding for designing advanced SACs.

1. Introduction

Single-atom catalysts (SACs) with maximized atom utilization efficiency have attracted significant attention due to their high catalytic activity and selectivity.^[1,2] These catalysts have been applied to CO oxidation,^[3,4] hydrogenation,^[5] dehydrogenation,^[6,7] and other electrochemical reactions.^[8,9] Significant effort has been devoted to obtaining a thorough understanding of SACs through unique characterization techniques and theoretical calculations.^[1,10–12]

Among the different types of SACs, Pt has been studied extensively for electrochemical reactions, especially the hydrogen evolution reaction (HER) and oxygen reduction reaction (ORR) in acidic media.^[10,13–16] For example, Liu et al. reported that the Pt single atoms on onion-

like nanospheres of carbon (Pt₁/OLC) showed improved catalytic activity in HER compared to Pt₁/graphene and commercial Pt/C. Theoretical calculations indicated that a tip-enhancement effect at the Pt site which induces strong localized electric fields may contribute to the activity for HER.^[17] Liu et al. reported that Pt single atoms supported on black porous carbon showed superior catalytic activity and stability for 4e⁻ ORR in acidic solution. The theoretical calculations indicated that the active sites of Pt SAC are single-pyridinic-nitrogen-atom-anchored Pt₁ atoms, which are highly active for ORR.^[14] Choi et al. demonstrated that the Pt single atoms supported on sulfur-doped zeolite-templated carbon (Pt/HSC) have high selectivity to the catalyze 2e⁻ ORR path and generate up to 96% hydroperoxide.^[16] Although many studies relating to the Pt SACs indicate that the unique electronic properties and local structures lead to superior performance in electrochemical reactions, there are gaps between the proposed theoretical models and the corresponding realistic behavior of the catalysts due to the limitations of ex-situ characterization. This has resulted in certain ambiguities surrounding the unique properties of Pt SACs and their potential application.

Currently, the observation of SACs catalysts under realistic reaction conditions is rare.^[9,10] In-situ characterization techniques, especially operando X-ray absorption spectroscopy (XAS), are promising methods to investigate the dynamic

J. Li, Dr. M. N. Banis, K. Adair, K. Davis, Dr. L. Zhang, Dr. F. Kong, R. Li, Prof. X. Sun

Department of Mechanical and Materials Engineering
University of Western Ontario
London, Ontario N6A 5B9, Canada
E-mail: xsun9@uwo.ca

Z. Ren, Prof. J. Luo
Center for Electron Microscopy and Tianjin Key Lab
of Advanced Functional Porous Materials
Institute for New Energy Materials and Low-Carbon Technologies
School of Materials Science and Engineering
Tianjin University of Technology
Tianjin 300384, China

D. M. Meira, Y. Z. Finfrock
CLS @ APS
Advanced Photon Source
Argonne National Laboratory
Lemont, IL 60439, USA

D. M. Meira, Y. Z. Finfrock
Science Division, Canadian Light Source Inc.
44 Innovation Boulevard, Saskatoon, Saskatchewan S7N 2V3, Canada

Prof. T. K. Sham
Department of Chemistry
University of Western Ontario
London, Ontario N6A 5B7, Canada

DOI: 10.1002/smll.202007245

electronic and local environment of these structures to unveil the nature of the active sites.^[18–23] Cao et al. successfully achieved atomically dispersed $\text{Fe}_1(\text{OH})_x$ on Pt nanoparticles (NPs), which showed 30 times higher mass activity than that of conventional catalysts and 100% CO selectivity over a wide temperature window for the preferential oxidation of CO in hydrogen. The in-situ XAS results showed the selective deposition of iron hydroxide on the surface of Pt NPs. The results illustrated that the interface of $\text{Fe}_1(\text{OH})_x/\text{Pt}$ can easily react with CO and facilitate oxygen activation.^[3] In addition, Cao and co-workers used operando XAS to study the formation of a high-valence $\text{HO-Co}_1\text{-N}_2$ moiety and successfully illustrated the formation of the reaction intermediate $\text{H}_2\text{O}-(\text{HO-Co}_1\text{-N}_2)$. Theoretical calculation results further confirmed that the highly oxidized and reconstructed Co_1 single atoms decreased the energy barrier for water dissociation, thus leading to the high catalytic performance of HER in alkaline media.^[24] Conducting operando XAS measurements can be difficult on SACs because of their low loading and poor stability in some reactions. These factors increase the difficulty in probing the local electronic and atomic structure of atoms engaged in the reaction, resulting in inaccurate and low-quality data.^[23] Although the in-situ/operando XAS measurements have been operated on SACs, the synthesis methods and types of support are not unified to achieve SACs, even the same metal element, thus could lead to ambiguous conclusions due to the methodology and support effects.

In this work, we reported that high loading Pt single atoms (2.0 wt%) on graphitic carbon nitride ($\text{g-C}_3\text{N}_4$) derived N-doped carbon nanosheets (NCNS) has been achieved by atomic layer deposition (ALD). Operando XAS were studied on Pt single atoms and NPs for both HER and ORR to gain a deeper understanding of this system. The operando results indicate that the total unoccupied density of states of Pt 5d orbitals of Pt_1 atoms is higher than that of Pt NPs under HER condition, which could be responsible for the high activity. And a stable Pt oxide is formed during ORR on Pt_1/NCNS , which may suppress the adsorption and activation of O_2 .

2. Results and Discussion

As shown in the **Figure 1a**, the NCNS were derived from $\text{g-C}_3\text{N}_4$, then carbonized with glucose by a hydrothermal method.^[25] The Pt_1/NCNS was achieved after performing one cycle of Pt ALD on the as-prepared NCNS, using trimethyl(methylcyclopentadienyl)platinum (IV) (MeCpPtMe_3) and O_2 as precursors. Higher deposition temperature (250 °C) and two cycles of Pt ALD were used to synthesize Pt NPs. Of note is that the presence of a small proportion of single atoms is hard to be avoided, therefore, we denoted the achieved Pt NPs as Pt-single atoms and NPs (SNs)/NCNS which represent the co-existence of Pt single atoms and NPs. The loadings of Pt on Pt_1/NCNS and Pt-SNs/NCNS were 2.0 and 7.5 wt%, respectively, calculated from inductively coupled plasma optical emission spectrometer (ICP–OES) results.

High-angle annular dark-field scanning transmission electron microscopy (HAADF-STEM) showed a uniform dispersion of Pt_1 atoms on the NCNS, without the presence of any visible NPs/clusters at both low- and high-magnifications (Figures 1b, 1c and Figure S1, Supporting Information). In the Pt-SNs/NCNS

sample, the size of the NPs was measured to be $\approx 1.6 \pm 0.2$ nm (Figures 1d, 1e and Figure S2, Supporting Information). X-ray diffraction patterns as shown in Figure S3, Supporting Information, present different diffraction patterns between $\text{g-C}_3\text{N}_4$ and NCNS, implying the decomposition of $\text{g-C}_3\text{N}_4$ and formation of NCNS through pyrolysis.^[25] However, no obvious Pt diffraction peaks can be found in the patterns, which can be attributed to the small size of Pt.^[26] To have better control over the deposition of high loading Pt SACs using ALD, it is necessary to identify and determine the effect of the controlling parameters in the synthesis process. Studies have shown that nitrogen defect sites in graphitic carbon play an important role in the deposition of Pt using ALD.^[27] NCNS with different proportions of N were prepared by controlling the hydrothermal temperatures. Interestingly, we found the Pt loadings achieved on the NCNS through ALD were highly dependent on the content of N in the NCNS, in which the loadings of Pt were 2.0, 0.7, and 0.5 wt% on the NCNS with 9.5, 8.0, and 5.4 at% N, respectively (Figure S4, Supporting Information). This solid evidence confirms the loadings of Pt are related to the N content and suggests that the Pt_1 atoms could bond with the N atoms through strong interactions.

Ex-situ XAS was carried out to characterize the electronic and structural properties of both Pt_1/NCNS and Pt-SNs/NCNS. It has been reported that the area under the whiteline (WL) peak in the Pt L_3 X-ray absorption near edge structure (XANES) spectra is directly related to the density of unoccupied Pt 5d orbitals.^[28] As shown in **Figure 2a**, the Pt_1/NCNS exhibited a much higher WL peak intensity than Pt-SNs/NCNS, indicating a higher fraction of unoccupied states in the 5d orbitals. Such a high oxidation state of Pt on Pt_1/NCNS indicates that the strong interaction between Pt single atoms and the substrate.^[7] The extended X-ray absorption fine structure (EXAFS) spectra are shown in Figure 2b. Both the Pt_1/NCNS and Pt-SNs/NCNS have a peak between 1.0 and 2.0 Å region in the radial distribution (Fourier Transform of the EXAFS, without phase correction), which can be attributed to the coordination of Pt-C/N/O. Another significant peak on Pt-SNs/NCNS can be found at 2.36 Å, which is the Pt-Pt coordination based on the Pt foil EXAFS result. No obvious Pt-Pt coordination can be found on Pt_1/NCNS , implying the atomically dispersed nature of the Pt single atoms. This observation is also consistent with the simple oscillation in the XANES region since the backscattering amplitude of the low atomic number of elements is linear in k space at the low k region, while the Pt back-scattering amplitude in k space is more complex and produces oscillation in the low k and mid k region (Figure 2a). Based on the EXAFS fitting results, the Pt_1 atom is likely bonded with approximately three or four C/N atoms at the ex-situ condition (Table S1, Supporting Information).

X-ray photoelectron spectroscopy (XPS) measurements were also carried out to investigate the valence state of the surface Pt. As shown in Figures 2c and 2d, the $\text{Pt } 4f_{7/2}$ binding energy peak on Pt_1/NCNS located at 73.2 eV is higher than that of Pt-SNs/NCNS (72.6 eV). Deconvolution of the XPS spectra showed that there are 60% Pt^{2+} and 40% metallic state Pt^0 , confirming the formation of NPs.^[29] However, a very symmetrical shape of spectrum was observed on Pt_1/NCNS (Figure 2c), which indicated that the Pt^{2+} species, suggesting positively charged Pt single atoms due to coordination with N or O atoms.^[30] This

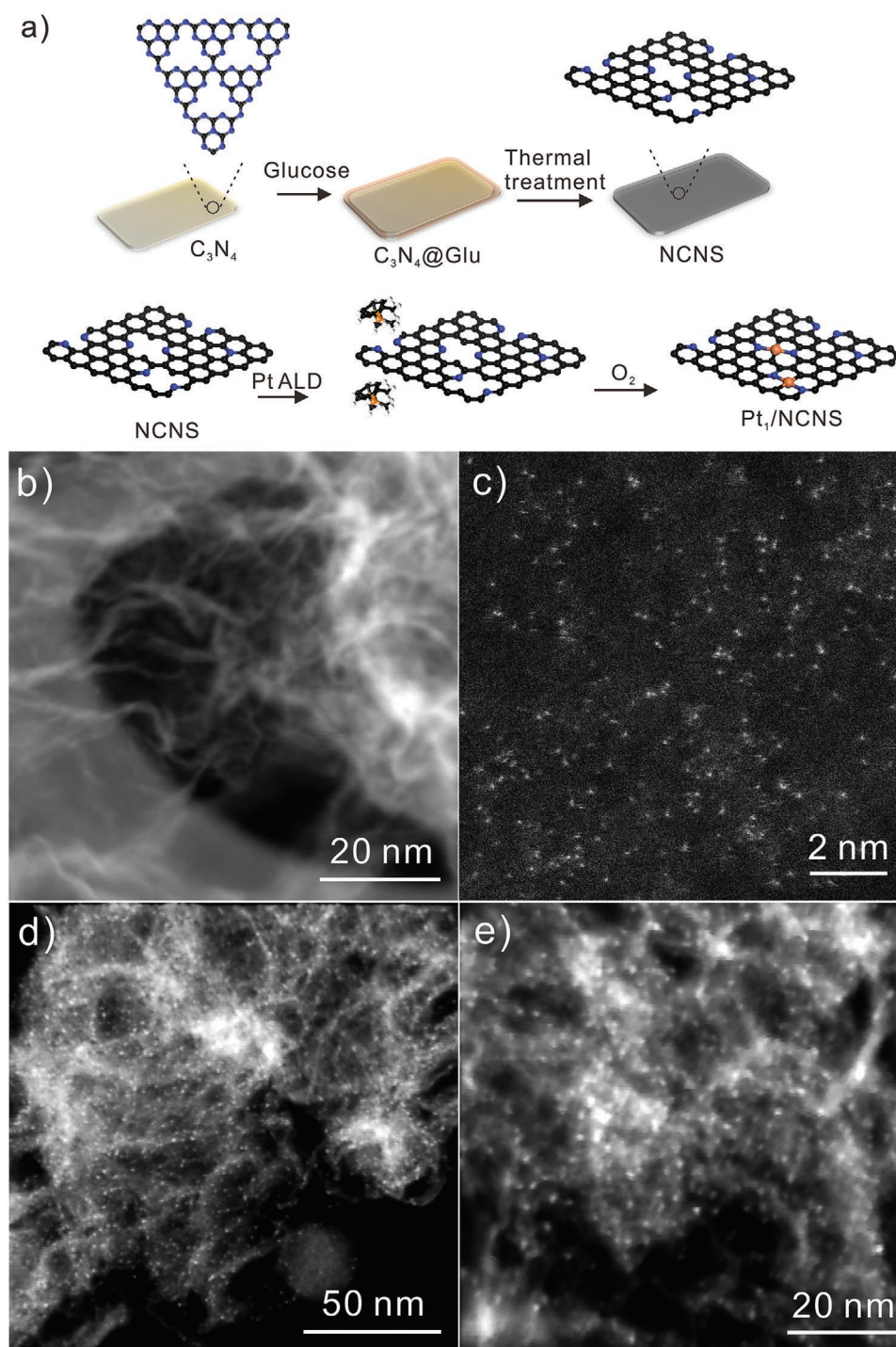


Figure 1. a) Illustration for the synthesis of Pt_1/NCNS . Representative aberration-corrected HAADF-STEM images of b,c) Pt_1/NCNS and d,e) Pt-SNs/NCNS. The black, blue, and orange spheres represent the C, N, and Pt atoms.

observation in XPS is in line with the ex-situ XANES results (Figure 2a). The lack of a metallic state Pt on Pt_1/NCNS also confirms the atomically dispersed structure of Pt single atoms.

The catalytic performance of Pt_1/NCNS and Pt-SNs/NCNS was characterized under HER and ORR conditions. As shown in Figure 3a, cyclic voltammograms were recorded in 0.5 M H_2SO_4 , which shows the hydrogen underpotential deposition

region, the double layer potential region, and the oxide formation potential region on the Pt-SNs/NCNS. However, only the double layer can be found on the Pt_1/NCNS , indicating that the lack of crystallized Pt NPs. As seen in Figure 3b, in HER, the Pt_1/NCNS displays a similar activity as Pt-NPs/NCNS with a much lower amount of Pt content. Further, calculated mass activity at the overpotential of 0.05 V—the Pt_1/NCNS showed a

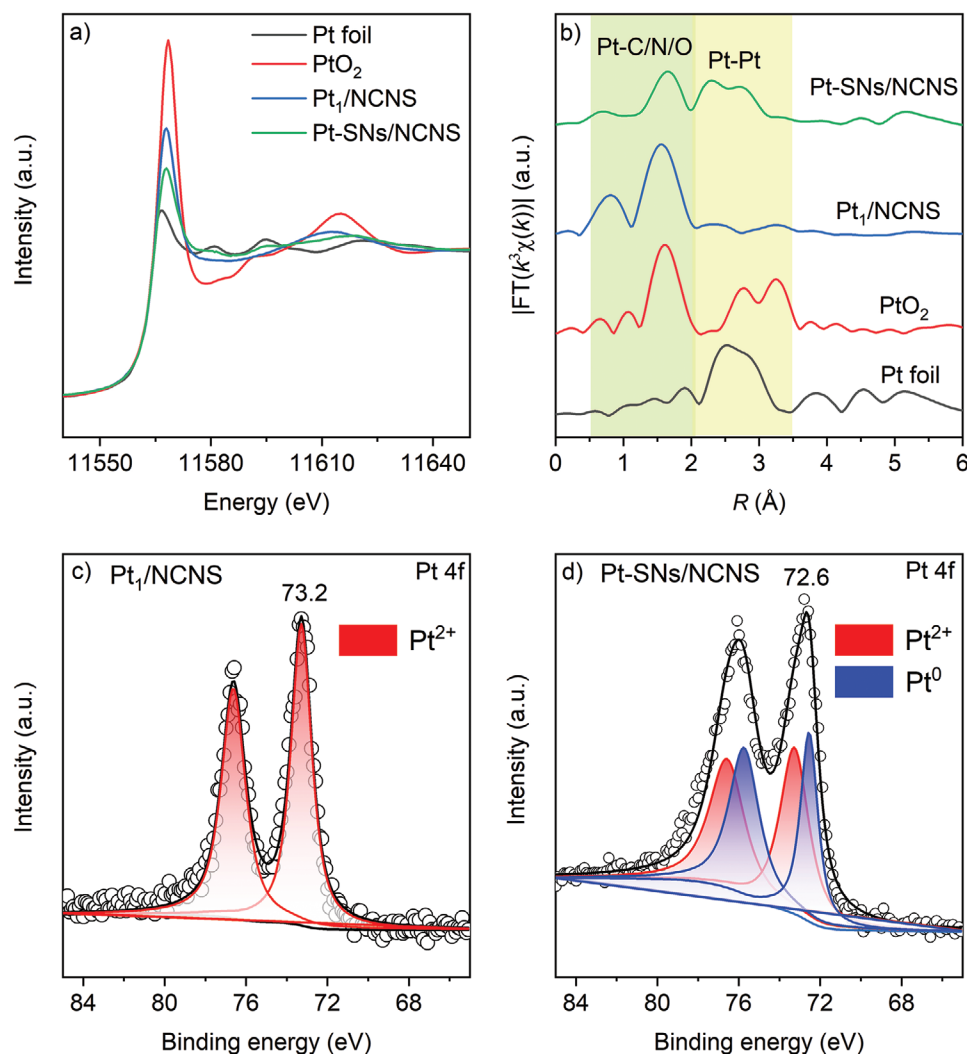


Figure 2. a) Ex-situ XANES and b) corresponding k^3 -weighted Fourier transform EXAFS spectra (No phase correction) spectra of Pt₁/NCNS and Pt-SNs/NCNS as well as the reference samples of Pt foil and PtO₂ at the Pt L₃-edge. c) XPS spectra of Pt₁/NCNS and d) Pt-SNs/NCNS in the Pt 4f region.

7.1 A mg⁻¹_{Pt} mass activity—is more than 4 times greater than that of the Pt-SNs/NCNS catalyst (1.6 A mg⁻¹) (Figure S5, Supporting Information), which is among the highest reported activity for Pt SACs in HER.^[8,31,32] The catalytic activity of Pt/C is lower than that of Pt-SNs/NCNS (Figure 3b and Figure S5a, Supporting Information), which could be because of the relatively larger size of Pt NPs on Pt/C. Based on the EXAFS results, the Pt₁ atom is likely bonded with approximately three or four C/N atoms (Table S1, Supporting Information). According to the reference, the hydrogen-adsorption free energies (ΔG_{H^*}) on Pt₁-C_xN_y ($x + y = 4$ or 3) are far away from zero, except that the Pt₁-C₂N₂ site and the two N atoms are in cross position, implying that the Pt₁-C₂N₂ should exhibit high catalytic activity in HER.^[33] Further analysis of the WL area of Pt₁/NCNS indicated that the Pt₁ atom could bond with two N atoms (Figure S6, Supporting Information).^[34] Taken together, the most possible configuration of Pt₁/NCNS could be Pt₁-C₂N₂ and the two N atoms are in cross position. The long-term stability tests of Pt₁/NCNS were carried out by applying a cyclic potential sweep between

−0.1 to 0.4 V for HER. Pt₁/NCNS shows ultra-stable activity even after 8000 cycles (Figure 3c), without showing obvious activity decline. However, in contrast with the results in HER, we found that the Pt-SNs/NCNS shows much better catalytic activity than Pt₁/NCNS in ORR (Figure 3d). The Pt-SNs/NCNS exhibits the onset potential (at 0.1 mA cm⁻²) at 1.02 V which is much higher than that of Pt₁/NCNS (0.71 V) (Figure S5, Supporting Information). The catalytic activities of Pt/C ORR is very close to that of Pt-SNs/NCNS (Figures 3d and Figure S5b, Supporting Information), indicating that the Pt NPs are dominantly on Pt-SNs/NCNS. The durability test under ORR reaction was also performed on Pt₁/NCNS at a cyclic potential sweep between 0.6 and 1.1 V at O₂ saturated 0.5 M H₂SO₄ for 5000 cycles. As shown in Figure 3e, the Pt₁/NCNS exhibits a good stability, without showing obvious decreased activity. A comparison of XANES (Figure S7, Supporting Information) and EXAFS (Figure 3f) spectra of the pristine and cycled Pt₁/NCNS in HER and ORR further demonstrate the high stability of Pt₁/NCNS. Moreover, the EXAFS fitting (Figure S8 and Tables S1 and S2, Supporting

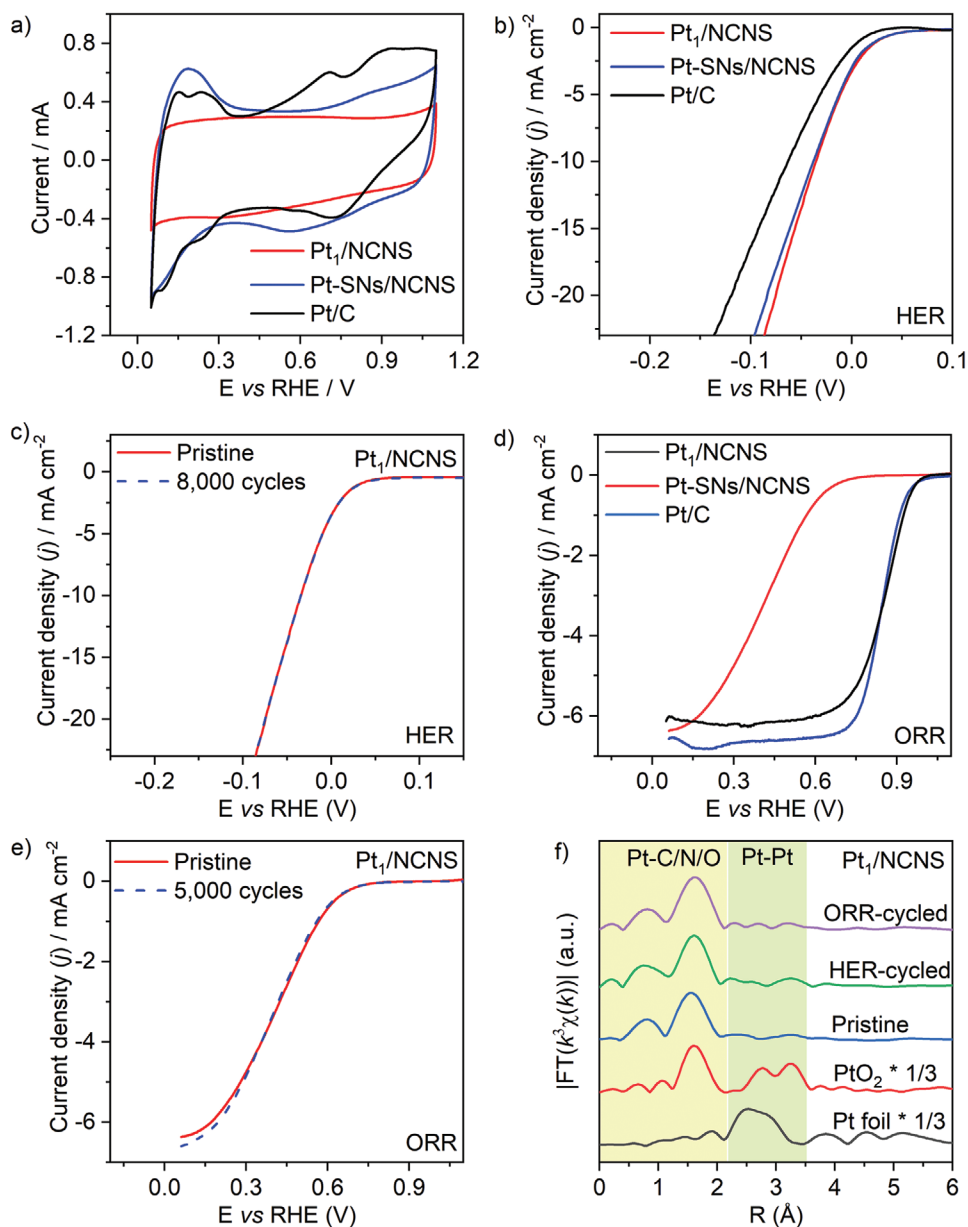


Figure 3. a) Cyclic voltammograms on Pt₁/NCNS, Pt-SNs/NCNS, and Pt/C catalysts. b) Polarization curves of Pt₁/NCNS, Pt-SNs/NCNS, and Pt/C in HER and c) the durability measurement on Pt₁/NCNS. d) Polarization curves of Pt₁/NCNS, Pt-SNs/NCNS, and Pt/C in ORR and e) the durability measurement on Pt₁/NCNS. f) EXAFS results of Pt₁/NCNS after durability tests.

Information), EDS-mapping, and HAADF-STEM (Figures S9 and S10, Supporting Information) results again confirm that the Pt₁/NCNS is stable under HER and ORR.

In order to reveal the nature of the active sites for both Pt₁/NCNS and Pt-SNs/NCNS in both HER and ORR as it happens, a custom-built electrochemical cell was used to perform an operando XAS. The Pt catalysts are coated on carbon paper as the working electrode (Figure S11, Supporting Information). The XAS spectrum was first taken at open circuit voltage (OCV). During the operando XAS measurements, the potential on the working electrode was decreased from 0.05 to -0.05 V versus RHE and 1.10 to 0.40 V versus RHE for HER and ORR, respectively.

In HER, with the applied potentials, the WL intensity of Pt₁/NCNS slightly decreases from OCV to -0.05 V (Figure 4a), while a larger decline on Pt-SNs/NCNS is observed (Figure 4c), indicating a lesser degree of changes in the total unoccupied density of states of Pt 5d orbitals on Pt₁/NCNS. Figure S12, Supporting Information, presents the k³-weighted Pt L₃-edge EXAFS spectra and the Fourier transform magnitudes of Pt₁/NCNS and Pt-SNs/NCNS (Figures 4b and 4d). As shown in Figure 4b, no obvious Pt-Pt coordination can be observed in all the Pt₁/NCNS operando EXAFS spectra, indicating that the Pt atoms were still singly dispersed under HER reaction. The main peak is found at 1.56 Å under OCV and 0.05 V, which is similar to the spectra collected in the ex-situ conditions, can

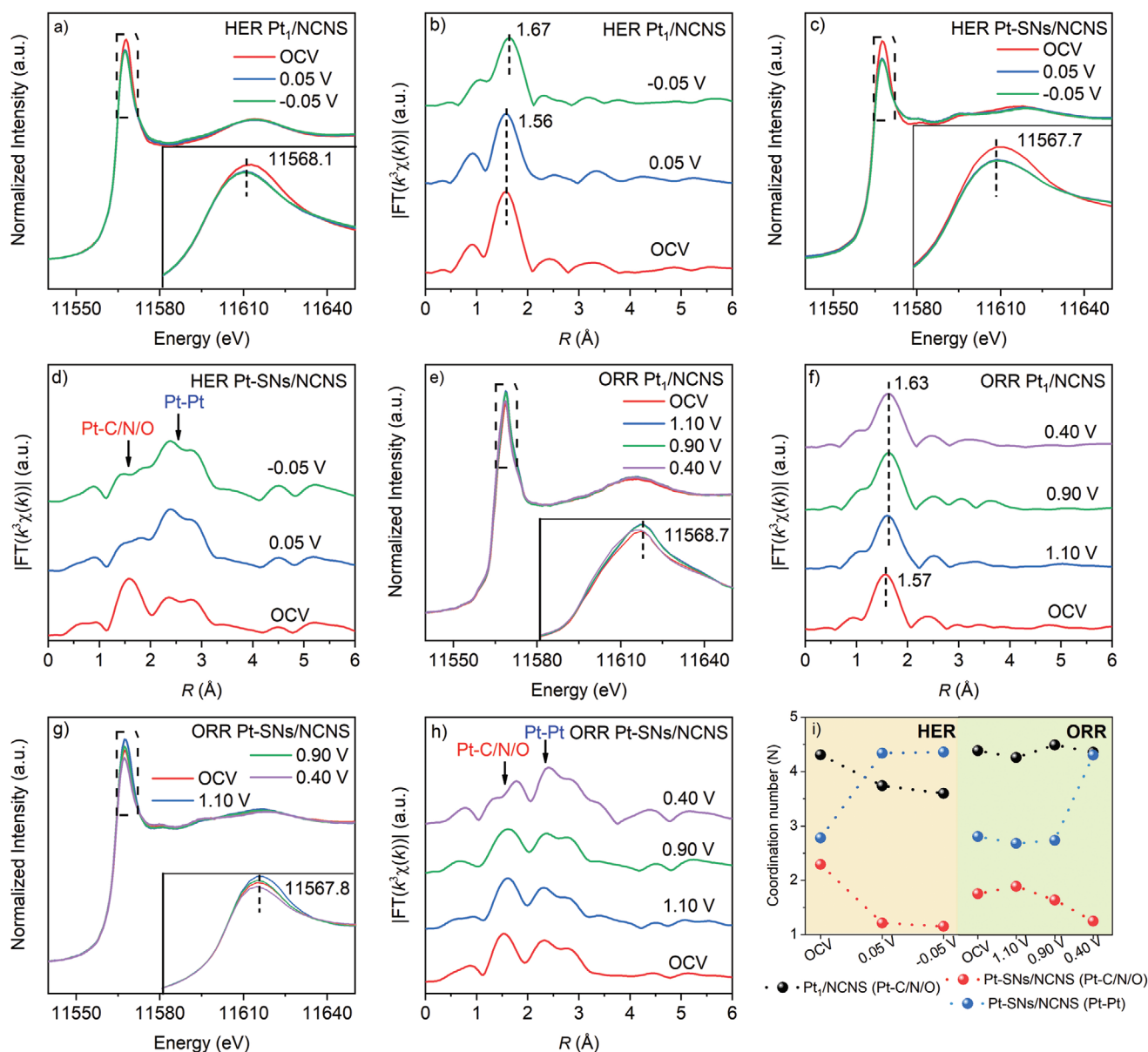


Figure 4. Operando XANES and EXAFS spectra at Pt L₃ edge for a,b) Pt₁/NCNS and c,d) Pt-SNs/NCNS at different applied voltages from open circuit condition to -0.05 V during electrocatalytic HER. Operando XANES and EXAFS spectra at Pt L₃ edge for e,f) Pt₁/NCNS and g,h) Pt-SNs/NCNS at different applied voltages from open circuit condition to 0.40 V during electrocatalytic ORR. Inset, zoom in area of WL region in dotted box. i) Coordination number of Pt₁/NCNS and Pt-SNs/NCNS under HER and ORR after quantitative EXAFS analysis.

be related to the coordination of Pt-C/N/O. When the potential decreased to -0.05 V, it shifts to 1.67 Å. This enlarged bonding distance (Table S1, Supporting Information) could be either due to the applied electric field or the adsorbed H* at the working potential, which causes the relaxation of the local structure of Pt₁ atoms. However, Pt-SNs/NCNS shows a distinct decrease of Pt-C/N/O coordination in the operando EXAFS results (Figure 4d). The Pt-Pt coordination increases on the Pt-SNs/NCNS when the potential was changed from OCV to -0.05 V, which indicates the reduction of the Pt oxide on Pt NPs.

After bubbling O₂ into the electrolyte for ORR, the position of WL peak on Pt₁/NCNS shifts to a higher energy (11 568.7 eV

(Figure 4e) compared with the corresponding XANES results in HER (Figure 4a), which can be due to the adsorption of O₂ on Pt₁/NCNS thus leading to a highly oxidized Pt species. With the applied potential decreased from 1.10 to 0.40 V, the intensities of the WL peak are almost unchanged on Pt₁/NCNS (Figure 4e). After Fourier transform (Figure S13, Supporting Information), the *k*³-weighted Pt L₃-edge EXAFS spectra of Pt₁/NCNS under ORR also show unobvious changes of the Pt-C/N/O coordination under ORR working conditions (Figure 4f). In contrast, as shown in Figure 4g, clearly the WL peak intensity decrease can be found on Pt-SNs/NCNS from 1.10 to 0.40 V. We also notice a gradually decreased Pt-C/N/O coordination but increased

Pt-Pt coordination from 1.10 to 0.40 V in the radial distribution (Figure 4h). Thus, the observation of XANES and EXAFS on Pt-SNs/NCNS in ORR indicates the reduction of Pt oxide.^[35]

In order to quantify the results, EXAFS curve-fittings were further performed (Figures S14–S17, Supporting Information) and the coordination number of Pt-C/N/O and Pt-Pt are shown in Figure 4i. Let us first focus on the HER; we find that the coordination number of Pt-C/N/O decreases from 4.31 to 3.60 on Pt₁/NCNS when the applied potential changed from OCV to –0.05 V (Table S1, Supporting Information), which can be ascribed to the desorption of H₂O.^[34] However, we found that the Pt-C/N/O coordination number decreases from 2.29 to 1.15 and this is accompanied by an increase in Pt-Pt coordination from 2.78 to 4.36 on the Pt-SNs/NCNS with the potential changed from OCV to –0.05 V. The trend of the coordination number of Pt-O and Pt-Pt indicates that the O/OH displacement occurred between the surface and bulk of Pt NPs.^[19,35] A comparison of Pt₁/NCNS and Pt-SNs/NCNS in terms of operando XANES results at –0.05 V is also shown in Figure S18, Supporting Information, regarding the catalytic activity differences in HER at this potential. A much higher WL intensity still can be found on the Pt₁/NCNS compared with Pt-SNs/NCNS even at the highly reduced condition in HER. This higher WL intensity indicates a higher total unoccupied density of states of Pt 5d orbitals in Pt₁/NCNS, which could be responsible for the highly catalytic activity.^[4,36] In ORR, the Pt-C/N/O coordination number on Pt₁/NCNS increases from 3.55 to 4.46 from the ex-situ to OCV and remains almost constant from 1.10 to 0.40 V. Because of the tied structure that Pt₁ atom bonds with four C/N atoms have, it is unlikely to be possible to form the fifth Pt-C/N bond. Therefore, the increased total coordination number of Pt-C/N/O on Pt₁/NCNS could be attributed to the adsorbed O₂ and generate the additional Pt-O path. Moreover, the total coordination numbers remain almost constant at 1.1 (4.35), 0.9 (4.55), and 0.4 V (4.43), indicating that the O₂ throughout adsorbs on Pt₁ atoms and form the stable PtO_x species (Table S2, Supporting Information). However, the Pt-C/N/O coordination number decreases from 2.28 to 1.72 and the Pt-Pt coordination number increases from 2.97 to 4.39 on the Pt-SNs/NCNS from 1.10 to 0.40 V. This observation on Pt-SNs/NCNS is entirely consistent with previous observations.^[19,35] A previous work indicated that the O₂ only physically adsorbs on the oxidized Pt₁ sites, which is very difficult for the O₂ activation.^[14] Based on our operando XAS results, the formation of stable Pt oxide species on Pt₁/NCNS may further decrease the possibility for O₂ adsorption and activation under ORR, which leads to their unsatisfied activity in ORR. However, the reduced surface of Pt NPs in Pt-SNs/NCNS could facilitate this process resulting in a higher activity of Pt-SNs/NCNS in ORR.

We further carried out the WL analysis to understand the changes of oxidation states of Pt on both Pt₁/NCNS and Pt-SN/NCNS under HER and ORR. As shown in Figure S19a–c, Supporting Information, when the potential applied at 0.05 V, the oxidation states decrease can be observed on both Pt₁/NCNS and Pt-SNs/NCNS compared with their ex-situ results in HER. However, we also found such decreasing on Pt-SNs/NCNS when the applied potential becomes more negative (–0.05 V), indicating that the further O/OH displacement occurred between the surface and bulk of Pt NPs, while the oxidation states of Pt on Pt₁/NCNS keep almost constant at these two

conditions. The higher total unoccupied density of states and atomic utilization efficiency Pt in Pt₁/NCNS contribute to its high catalytic activity in HER.

Under ORR conditions, we noticed that both the Pt₁/NCNS and Pt-SNs/NCNS show increased oxidation states from +2.40 to +2.42 and +1.23 to +1.42, respectively, from the ex-situ to 1.1 V (Figure S19d–f, Supporting Information). When the applied potentials negatively shift to 0.4 V, the oxidation states of Pt on Pt-SNs/NCNS decrease from +1.42 to +0.94, indicating the consumption of PtO_x on Pt NPs. However, with the same applied overpotential, the oxidation states of Pt on Pt₁/NCNS only decrease from +2.42 to +2.37, which is close to its ex-situ result (+2.40). The EXAFS fitting results (Table S2, Supporting Information) further indicated that additional Pt-C/N/O coordination occurs on Pt₁/NCNS under the ORR condition. This observation unambiguously indicated that the stable PtO_x species is formed on Pt₁/NCNS, which could suppress the activation of O₂ thus leading to the relatively lower catalytic activity of Pt₁/NCNS in ORR.

3. Conclusion

In conclusion, we have successfully achieved a high loading Pt₁/NCNS SAC through ALD. The HAADF-STEM, XAS, and XPS demonstrated the presence of singly dispersed Pt₁ atoms. The operando XAS results indicated that the total unoccupied density of states of Pt 5d orbitals of Pt₁ atoms is higher than that of Pt NPs in HER, while a stable Pt oxide is formed during ORR on Pt₁/NCNS which may suppress the adsorption and activation of O₂. This work provides new insight into Pt SACs and unveils the nature of Pt single atoms under realistic HER and ORR conditions, which improves understanding for the synthesis of advanced SACs.

4. Experimental Section

See the details in the Supporting information.

Supporting Information

Supporting Information is available from the Wiley Online Library or from the author.

Acknowledgements

J.L. and M.N.B. contributed equally to this work. This work was supported by the Natural Sciences and Engineering Research Council of Canada (NSERC), Ballard Power Systems, Canada Research Chair (CRC) Program, Canada Foundation for Innovation (CFI), the University of Western Ontario, and the 111 project of China (D17003). J.L. was supported by the China Scholarship Council (CSC). This research used resources of the Advanced Photon Source, an Office of Science User Facility operated for the U.S. Department of Energy (DOE) Office of Science by Argonne National Laboratory and was supported by the U.S. DOE under Contract No. DE-AC02-06CH11357, and the Canadian Light Source and its funding partners. The authors also would like to thank Dr. Timothy Fister for the use of the electrochemical workstation during

the operando experiments at APS. The authors would like to thank Dr. Ning Chen at HXMA beamlines of Canadian Light Source (CLS) for the great help on the XAS measurements.

Conflict of Interest

The authors declare no conflict of interest.

Data Availability Statement

The data that support the findings of this study are available from the corresponding author upon reasonable request.

Keywords

atomic layer deposition, hydrogen evolution reaction, operando X-ray absorption spectroscopy, oxygen reduction reaction, single-atom catalysts

Received: November 17, 2020

Revised: December 30, 2020

Published online:

- [1] X. F. Yang, A. Q. Wang, B. T. Qiao, J. Li, J. Y. Liu, T. Zhang, *Acc. Chem. Res.* **2013**, *46*, 1740.
- [2] J. Guo, J. Huo, Y. Liu, W. Wu, Y. Wang, M. Wu, H. Liu, G. Wang, *Small Methods* **2019**, *3*, 1900159.
- [3] L. N. Cao, W. Liu, Q. Q. Luo, R. T. Yin, B. Wang, J. Weissenrieder, M. Soldemo, H. Yan, Y. Lin, Z. H. Sun, C. Ma, W. H. Zhang, S. Chen, H. W. Wang, Q. Q. Guan, T. Yao, S. Q. Wei, J. L. Yang, J. L. Lu, *Nature* **2019**, *565*, 631.
- [4] B. Qiao, A. Wang, X. Yang, L. F. Allard, Z. Jiang, Y. Cui, J. Liu, J. Li, T. Zhang, *Nat. Chem.* **2011**, *3*, 634.
- [5] H. Yan, H. Cheng, H. Yi, Y. Lin, T. Yao, C. Wang, J. Li, S. Wei, J. Lu, *J. Am. Chem. Soc.* **2015**, *137*, 10484.
- [6] H. Yan, Y. Lin, H. Wu, W. H. Zhang, Z. H. Sun, H. Cheng, W. Liu, C. L. Wang, J. J. Li, X. H. Huang, T. Yao, J. L. Yang, S. Q. Wei, J. L. Lu, *Nat. Commun.* **2017**, *8*, 1070.
- [7] J. Li, Q. Guan, H. Wu, W. Liu, Y. Lin, Z. Sun, X. Ye, X. Zheng, H. Pan, J. Zhu, *J. Am. Chem. Soc.* **2019**, *141*, 14515.
- [8] N. Cheng, S. Stambula, D. Wang, M. N. Banis, J. Liu, A. Riese, B. Xiao, R. Li, T. K. Sham, L. M. Liu, G. A. Botton, X. Sun, *Nat. Commun.* **2016**, *7*, 13638.
- [9] Y. Chen, S. Ji, C. Chen, Q. Peng, D. Wang, Y. Li, *Joule* **2018**, *2*, 1242.
- [10] L. Zhang, K. Doyle-Davis, X. L. Sun, *Energy Environ. Sci.* **2019**, *12*, 492.
- [11] B. Zhang, G. Sun, S. Ding, H. Asakura, J. Zhang, P. Sautet, N. Yan, *J. Am. Chem. Soc.* **2019**, *141*, 8185.
- [12] M. Zhou, S. Bao, A. J. Bard, *J. Am. Chem. Soc.* **2019**, *141*, 10117.
- [13] M. Li, K. Duanmu, C. Wan, T. Cheng, L. Zhang, S. Dai, W. Chen, Z. Zhao, P. Li, H. Fei, Y. Zhu, R. Yu, J. Luo, K. Zang, Z. Lin, M. Ding, J. Huang, H. Sun, J. Guo, X. Pan, W. A. Goddard, P. Sautet, Y. Huang, X. Duan, *Nat. Catal.* **2019**, *2*, 495.
- [14] J. Liu, M. Jiao, L. Lu, H. M. Barkholtz, Y. Li, Y. Wang, L. Jiang, Z. Wu, D.-J. Liu, L. Zhuang, C. Ma, J. Zeng, B. Zhang, D. Su, P. Song, W. Xing, W. Xu, Y. Wang, Z. Jiang, G. Sun, *Nat. Commun.* **2017**, *8*, 15938.
- [15] S. Yang, J. Kim, Y. J. Tak, A. Soon, H. Lee, *Angew. Chem., Int. Ed.* **2016**, *55*, 2058.
- [16] C. H. Choi, M. Kim, H. C. Kwon, S. J. Cho, S. Yun, H.-T. Kim, K. J. Mayrhofer, H. Kim, M. Choi, *Nat. Commun.* **2016**, *7*, 10922.
- [17] D. Liu, X. Li, S. Chen, H. Yan, C. Wang, C. Wu, Y. A. Haleem, S. Duan, J. Lu, B. Ge, P. M. Ajayan, Y. Luo, J. Jiang, L. Song, *Nat. Energy* **2019**, *4*, 512.
- [18] J. Dou, Z. Sun, A. A. Opalade, N. Wang, W. Fu, F. Tao, *Chem. Soc. Rev.* **2017**, *46*, 2001.
- [19] D. Friebe, D. J. Miller, C. P. O'Grady, T. Anniyev, J. Bargar, U. Bergmann, H. Ogasawara, K. T. Wikfeldt, L. G. M. Pettersson, A. Nilsson, *Phys. Chem. Chem. Phys.* **2011**, *13*, 262.
- [20] M. N. Banis, H. Yadegari, Q. Sun, T. Regier, T. Boyko, J. G. Zhou, Y. M. Yiu, R. Y. Li, Y. F. Hu, T. K. Sham, X. L. Sun, *Energy Environ. Sci.* **2018**, *11*, 2073.
- [21] J. Zhang, Y. Zhao, X. Guo, C. Chen, C.-L. Dong, R.-S. Liu, C.-P. Han, Y. Li, Y. Gogotsi, G. Wang, *Nat. Catal.* **2018**, *1*, 985.
- [22] Y. Lu, J. Wang, L. Yu, L. Kovarik, X. Zhang, A. S. Hoffman, A. Gallo, S. R. Bare, D. Sokaras, T. Kroll, V. Dagle, H. Xin, A. M. Karim, *Nat. Catal.* **2019**, *2*, 149.
- [23] C. Dessal, T. Len, F. Morfin, J.-L. Rousset, M. Aouine, P. Afanasiev, L. Piccolo, *ACS Catal.* **2019**, *9*, 5752.
- [24] L. L. Cao, Q. Q. Luo, W. Liu, Y. K. Lin, X. K. Liu, Y. J. Cao, W. Zhang, Y. Wu, J. L. Yang, T. Yao, S. Q. Wei, *Nat. Catal.* **2019**, *2*, 134.
- [25] H. Yu, L. Shang, T. Bian, R. Shi, G. I. Waterhouse, Y. Zhao, C. Zhou, L. Z. Wu, C. H. Tung, T. Zhang, *Adv. Mater.* **2016**, *28*, 5080.
- [26] J. Jones, H. Xiong, A. T. DeLaRiva, E. J. Peterson, H. Pham, S. R. Challa, G. Qi, S. Oh, M. H. Wiebenga, X. I. P. Hernández, *Science* **2016**, *353*, 150.
- [27] S. Stambula, N. Gauquelin, M. Bugnet, S. Gorantla, S. Turner, S. H. Sun, J. Liu, G. X. Zhang, X. L. Sun, G. A. Botton, *J. Phys. Chem. C* **2014**, *118*, 3890.
- [28] F. W. Lytle, *J. Catal.* **1976**, *43*, 376.
- [29] Y. Lykhach, A. Bruix, S. Fabris, V. Potin, I. Matolínová, V. Matolín, J. Libuda, K. M. Neyman, *Catal. Sci. Technol.* **2017**, *7*, 4315.
- [30] Y. Q. Zhu, T. Cao, C. B. Cao, J. Luo, W. X. Chen, L. R. Zheng, J. C. Dong, J. Zhang, Y. H. Han, Z. Li, C. Chen, Q. Peng, D. S. Wang, Y. D. Li, *ACS Catal.* **2018**, *8*, 10004.
- [31] Z. Q. Zhang, Y. G. Chen, L. Q. Zhou, C. Chen, Z. Han, B. S. Zhang, Q. Wu, L. J. Yang, L. Y. Du, Y. F. Bu, P. Wang, X. Z. Wang, H. Yang, Z. Hu, *Nat. Commun.* **2019**, *10*, 1657.
- [32] S. Ye, F. Luo, Q. Zhang, P. Zhang, T. Xu, Q. Wang, D. He, L. Guo, Y. Zhang, C. He, *Energy Environ. Sci.* **2019**, *12*, 1000.
- [33] J. N. Tiwari, S. Sultan, C. W. Myung, T. Yoon, N. Li, M. Ha, A. M. Harzandi, H. J. Park, D. Y. Kim, S. S. Chandrasekaran, *Nat. Energy* **2018**, *3*, 773.
- [34] S. Fang, X. Zhu, X. Liu, J. Gu, W. Liu, D. Wang, W. Zhang, Y. Lin, J. Lu, S. Wei, Y. Li, T. Yao, *Nat. Commun.* **2020**, *11*, 1029.
- [35] K. Sasaki, N. Marinkovic, H. S. Isaacs, R. R. Adzic, *ACS Catal.* **2016**, *6*, 69.
- [36] P. P. Hu, Z. W. Huang, Z. Amghouz, M. Makkee, F. Xu, F. Kapteijn, A. Dikhtiarenko, Y. X. Chen, X. Gu, X. F. Tang, *Angew. Chem., Int. Ed.* **2014**, *53*, 3418.